

**Highlights:**

- The corrosion resistance of PEO coatings was enhanced by facile sealing treatment.
- Ca containing precipitate was deposited on the coating surface.
- The existence of SDS provides hydrophobicity and inhibition effect for the coating.
- Increased hydrophobicity has negative influence on the paint adhesion of the coating.

## Ca-based sealing of plasma electrolytic oxidation coatings on AZ91 Mg alloy

Xiaopeng Lu<sup>1\*</sup>, Jirui Ma<sup>1</sup>, Marta Mohedano<sup>2\*</sup>, Borja Pillado<sup>2</sup>, Raúl Arrabal<sup>2</sup>, Kun Qian<sup>3</sup>, Yan Li<sup>1</sup>, Tao Zhang<sup>1</sup>, Fuhui Wang<sup>1</sup>

<sup>1</sup>Shenyang National Laboratory for Materials Science, Northeastern University, 3-11 Wenhua Road, Shenyang, 110819, China

<sup>2</sup>Departamento de Ingeniería Química y de Materiales, Facultad de Ciencias Químicas, Universidad Complutense, 28040 Madrid, Spain

<sup>3</sup>School of Materials Science and Engineering, Southeastern University, Nanjing, 211189, China

\*Corresponding authors: Dr. Xiaopeng Lu (luxiaopeng@mail.neu.edu.cn), Dr. Marta Mohedano (mmohedan@ucm.es)

**Abstract:** Plasma electrolytic oxidation (PEO) coatings on AZ91 Mg alloy were sealed in calcium nitrate solutions at different pH values (3, 4 and 5). Sodium dodecyl sulfate (SDS) was added to study the effect of SDS on the corrosion resistance of the sealed coatings. The microstructure, chemical composition and corrosion resistance of the coatings were investigated by means of SEM, XPS, XRD and electrochemical corrosion tests. The corrosion performance of the coatings was improved due to precipitation of Ca-containing precipitate. Low pH and SDS addition enhanced hydroxyapatite precipitation and produced hydrophobic coatings with worse paint adhesion but better corrosion resistance.

**Keywords:** Magnesium; Plasma electrolytic oxidation; Sealing; Corrosion resistance

### 1. Introduction

Plasma electrolytic oxidation (PEO) is an environmental-friendly surface treatment process that has shown advantages to enhance both corrosion and wear resistance of Mg alloys [1-6]. The technique involves polarization at high voltages (i.e. above dielectric breakdown) resulting in short-lived micro discharges and development of ceramic-like layer. The phase composition of the coating is mainly originated from the substrate and electrolyte [7-9]. However, porosity formed due to gas evolution at the location of the high-intensity discharges severely compromises the coating corrosion performance [10, 11].

Sealing of the porous layer by post-treatment has been explored as an alternative to improve the long-term corrosion resistance of PEO coated Mg alloy. Sol-gel [12-14],

epoxy [15-18] and inorganic coatings [19-23] are examples of strategies aimed at forming additional layers or blocking the coating pores and defects. As a general rule, when compared with organic sealings, inorganic based post-treatments are easier to apply, more environmentally friendly and show better thermal and mechanical integrity [24]. The adhesion of polymer based top layers also tends to be higher in case of inorganic sealings, although new hybrid systems based on organic sealings can provide a good adhesive based for organic coatings [18, 25, 26]. As can be observed in Table 1, sealing of PEO coated Mg by means of immersion into inorganic solutions appears to be an efficient and facile way for industrial application. It was recently found that optimized Ce-based treatment can improve the corrosion performance of PEO coatings by sealing the open pores with precipitation product. However, the acidic electrolyte used during post-treatment process may lead to excessive coating dissolution and deterioration of the inner barrier layer [19, 20, 22]. Mingo et al. [27] investigated the sealing effect of three different post-treatment processes on the corrosion property of PEO coatings on AZ91 Mg alloy. It was reported that coating sealed by octadecylphosphate acid (ODP) showed the best corrosion performance because of the hydrophobic property.

Corrosion inhibitors for Mg alloys are being studied extensively due to their promising results [28-32]. In this sense, it is worth noting that the high porosity of PEO coatings can be regarded as a natural container for storing corrosion inhibitors [14, 31, 33, 34]. For instance, Yang et al. [33] added 3-methysalicylate via low vacuum environment and subsequently sealed the PEO coating by dip-coating in an epoxy resin. They found that the electrochemically active areas and corrosion current density were reduced to relatively low levels after incorporation of corrosion inhibitor. Therefore, loading of corrosion inhibitors into the porous PEO layer is feasible and may constitute a viable means to achieve active corrosion protection.

In the present study, Ca-based sealing post-treatment was applied to seal the porous PEO coating formed on AZ91 Mg alloy for structural applications. Since the dissolution/precipitation reaction during sealing is of vital importance for the coating properties, the effects of pH during post-treatment were studied on the morphology, composition and corrosion resistance of PEO coatings. Sodium dodecyl sulfate (SDS), which was previously found to be an effective corrosion inhibitor for AZ91 Mg [35, 36], was evaluated as an additive for improving the sealing performance.

## 2. Material and methods

### 2.1 Materials and coating preparation process

AZ91 Mg alloy in size of 30×15×5mm was ground up to 2000 grit SiC paper before fabrication of PEO coatings. The chemical composition of the alloy can be found in our previous study [37]. The PEO specimens were produced in an alkaline phosphate containing electrolyte (30 g/L  $\text{Na}_3\text{PO}_4 \cdot 12 \text{H}_2\text{O}$ , 4 g/L  $\text{KF} \cdot 2 \text{H}_2\text{O}$  and 2 g/L NaOH) under a galvanostatic current mode ( $2 \text{ A/cm}^2$ ) for 15 min. The applied frequency was 500 Hz and duty ratio was 30%. The post-treatment solution was composed of 70 g/L  $\text{Ca}(\text{NO}_3)_2$ , which was adjusted to different pH values (3, 4 and 5) by dripping diluted nitric acid. 0.1 mol/L SDS was added to the post-treatment electrolytes to investigate the influence of corrosion inhibitor on the corrosion resistance of the coatings. Each post-treatment process was carried out in  $\text{Ca}(\text{NO}_3)_2$  containing solution at 80 °C for 60 min. The coatings were identified with the acronyms PPEO (blank PEO coating), PPEO-Ca-pH3, PPEO-Ca-pH4, PPEO-Ca-pH5, PPEO-Ca-pH3-SDS, PPEO-Ca-pH4-SDS and PPEO-Ca-pH5-SDS, which specify the pH of the Ca-containing solution and the addition of SDS as required. All reagents used in this study were purchased from Macklin Biochemical Co., Ltd, China.

### 2.2 Characterization of the coatings

The surface and cross section of the coatings were examined by using scanning electron microscopy/energy-dispersive X-ray microanalysis (JEOL JSM-6400 instrument). Cross section of the coatings was prepared by embedding the coatings in a commercial epoxy resin (EpoFix kit-Struers), followed by grinding through successive grades of SiC paper. The embedded samples were finally polished with 1  $\mu\text{m}$  diamond paste. Phase composition of the coatings was studied by X-ray diffraction (XRD) using a Philips X'Pert diffractometer ( $\text{Cu K}\alpha = 1.54056 \text{ \AA}$ , Bragg-Brentano configuration,  $0.5^\circ$  grazing angle and  $2\theta$  range from  $10^\circ$  to  $90^\circ$ ). The coating surface was further analyzed by X-ray photoelectron spectroscopy (XPS). XPS measurements were carried out with a monochromatic Al  $K\alpha$  (1486.6 eV) instrument. The samples were etched for 1 min by argon ion to remove contamination on the coating surface. Peak identification was carried out by using XPSpeak41 software and the binding energy was calibrated to C1s (284.6 eV) peak.

### 2.3 Corrosion measurements

Electrochemical corrosion tests were carried out using a computer controlled potentiostat (Princeton Instruments P4000) in 3.5 wt.% NaCl solution. A traditional three-electrode cell consisting of PEO specimen as the working electrode, saturated calomel electrode as reference electrode and platinum sheet as counter electrode. After immersion for 30 minutes, potentiodynamic polarization was scanned from open circuit potential (OCP) in a rate of 0.333 mV/s to anodic and cathodic direction, separately (the scan range was at least 300 mV in each direction). Electrochemical impedance spectroscopy (EIS) was carried out from  $10^5$  to  $10^{-2}$  Hz with a perturbation amplitude of 20 mV (peak-to-peak) sinusoidal perturbation. The obtained data were analyzed by ZsimpWin software. The chi-squared of the fitting was less than 0.01. All measurements were repeated at least for three times to guarantee the repeatability.

## 2.4 Contact angle measurement

Static contact angle test was performed using deionized water under ambient conditions using an FTA1000 Drop Shape Analysis System (First Ten Angstroms). The values reported are the average of 6 measurements in two different specimens (3 drops each).

## 2.5 Dry paint adhesion test

Measurements were conducted based on ISO 2409 standard. Paint and epoxy primer 37076 were supplied by AkzoNobel and various components were applied and mixed following the technical data sheet. The paint layer about  $21 \pm 2$   $\mu\text{m}$  thickness was obtained after specimens were cured 1 hour at 80 °C. After the test, specimens were rated based on the detached surface (%) from 0 (no detachment) to 5 (complete detachment).

# 3. Results and discussion

## 3.1 Coating characterization

Fig. 1 and 2 demonstrate the surface and cross section of the coatings before and after the different sealing treatments. Open pores in size of 2-5  $\mu\text{m}$  and cracks can be observed on the coating surface, which is typical microstructure for PEO coated Mg (Fig. 1a) generated due to gas evolution and discharges during coating formation process [38]. It is apparent that the surface of all PEO coatings is partially covered by newly formed precipitates after the sealing post-treatments. Precipitation is more prominent for lower pH values and in the presence of SDS, suggesting that coating or substrate dissolution under relatively acidic conditions plays a vital role in the sealing

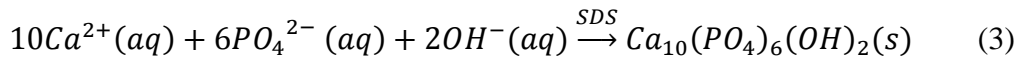
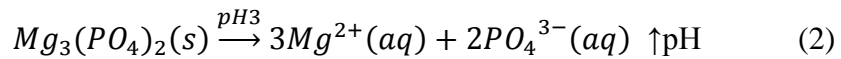
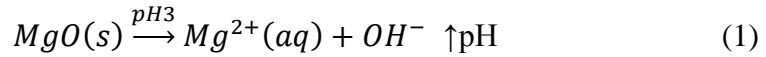
process. The effect of SDS on the reaction/precipitation process is quite significant as seen in the PPEO-Ca-pH3-SDS specimen, which is completely covered by Ca-rich deposits. It is difficult to distinguish the initial crater-like morphology and microcracks of the initial PEO coating (Fig. 1e-f).

As shown in Fig. 2, the post-treatment has a slight influence on the coating thickness, being  $\sim 20\text{ }\mu\text{m}$  for all specimens. The coatings reveal a double-layered microstructure with a porous outer part (pores being smaller near the substrate) and a dense micrometer-thick barrier layer adjacent to the substrate. Some of the open pores are partially filled with precipitates in the sealed specimens. Although chemical reaction occurs as reflected by the sealed pores, the original coating is partially dissolved in the acidic electrolyte, leading to redeposition and sealing of the pores on the coating surface. Therefore, the coating thickness is not significantly affected and is balanced by the dissolution and redeposition speed during the post-treatment process. In Fig. 3, it can be observed that the Ca signal is more evident for the specimens sealed in the presence of SDS (Fig. 3). It is worth noting that the location of the Ca-rich deposits is also observed in the optical micrographs due to preferential adsorption or contamination of the blue dye-containing lubricant that was used for polishing (attempts to remove this contamination by ultrasonic cleaning were unsuccessful).

The chemical composition of the coatings before and after sealing treatment can be found in Table 2. The initial coating is mainly composed of O, Mg, P and F. After the sealing post-treatments Mg and F contents are reduced while O levels increase. As expected, Ca is detected on the sealed surfaces, particularly when SDS is introduced into the sealing treatment solution. The concentration of P on the coating surface is slightly influenced by the sealing treatment.

MgO peaks and a broad amorphous peak in the  $20\text{--}35^\circ$  range are the most distinct features in the XRD patterns (Fig. 4). This suggests that P is incorporated into an amorphous phase within the coating.  $\text{MgF}_2$  compound was also identified in the particular case of PPEO coating, which might indicate its possible dissolution during post-treatments. Peaks corresponding to hydroxyapatite,  $\text{Ca}_{10}(\text{PO}_4)_6(\text{OH})_2$ , were also detected in the PPEO-Ca-pH3-SDS specimen. It can be inferred that the redeposition process of the Ca containing precipitate (hydroxyapatite) is controlled by the dissolution and redeposition speed during the post-treatment process. The sealing mechanism of the  $\text{Ca}(\text{NO}_3)_2$  based electrolyte is associated with the balance of

dissolution/precipitation process during post-treatment, where the original coating is dissolved in the acidic post-treatment electrolyte, resulting in increase of the pH locally (Equation 1 and 2). The increases of the pH initiate the reaction between  $\text{Ca}^{2+}$  and phosphate ions (Equation 3). It was reported that SDS can be used to facilitate synthesis of hydroxyapatite [39]. Therefore, the presence of SDS and lower pH of the post-treatment electrolyte lead to formation of more amounts of hydroxyapatite on the coating surface.



The survey XPS spectra and high-resolution Ca 2p, P 2p and S 2p spectra of the post-treated coatings are shown in Fig. 5. Findings confirm  $\text{Ca}_{10}(\text{PO}_4)_6(\text{OH})_2$  as the main Ca-containing compound on the sealed surfaces as evidenced by the Ca peak located at 347.1 eV (Fig. 5b and c) [40]. The binding energy of P 2p (Fig. 5d and e) at 131.5 eV corresponds to  $\text{PO}_4^{3-}$  and 133.3 eV can be assigned to  $\text{HPO}_4^{2-}$  [41, 42]. SDS is also detected on the coating surface after sealing post-treatment process. The spectrum of S 2p (Fig. 5f) is attributed to  $-\text{SO}_4^{2-}$  [43].

### 3.2 Corrosion performance of the coatings

The corrosion resistance of the coatings was evaluated by performing polarization test in 3.5 wt. % NaCl solution at room temperature (Fig. 6 and Table 3). It can be seen that the polarization curves are shifted to lower current densities and higher potentials for all the sealed coatings. The calculated corrosion current density ( $i_{\text{corr}}$ ) of the unsealed coating is  $0.57 \mu\text{A}/\text{cm}^2$ , whereas the  $i_{\text{corr}}$  of the coatings after post-treatment decreases by one order of magnitude. The lowest values were found for the coatings sealed in the presence of SDS. It is also worth noticing that the slope changes in the anodic branches (i.e. breakdown potentials) are higher in case of sealed specimens, indicating an improved passivation of the surfaces.

EIS measurements were performed to investigate the long-term corrosion performance of the coatings, as shown in Fig. 7 and 8. According to the Nyquist plots, PEO-Ca-pH3-SDS and PEO-Ca-pH4-SDS show a large capacitive loop at low frequencies (Fig. 7a and b), indicating superior corrosion resistance versus the coatings without

corrosion inhibitor. It can be seen in the Bode plots in Fig. 7c that the impedance modulus ( $|Z|$ ) in the low frequency range increased significantly after sealing treatment. This enhancement was more noticeable for the coatings with the addition of corrosion inhibitor, which also show an additional time constant. The phase angle of PEO-Ca-pH3-SDS is close to  $90^\circ$ , suggesting that the open pores of the layer are blocked by SDS as well as by hydroxyapatite. It is worth mentioning that hydroxyapatite is more stable than MgO at neutral pH, thus enhancing the performance of the PEO coating in 3.5 wt.% NaCl solution. In Fig. 8, the impedance values at low frequency decrease by one order of magnitude for all samples after 120 h immersion test, although the impedance of the sealed coatings is still higher than that of the unsealed coating. Equivalent circuits were used to fit the obtained EIS data (Fig. 9).  $R_s$  represents the resistance of NaCl solution,  $R_{Ca}$  and  $CPE_{Ca}$  are the corrosion resistance and capacitance of the Ca-rich layer.  $R_{PEO}$  and  $CPE_{PEO}$  are the corrosion resistance and capacitance of the porous PEO coating.  $CPE_{dl}$  and  $R_{ct}$  are related to the double layer capacitance and charge transfer resistance at the metal/electrolyte interface. The fitted electrochemical parameters are summarized in Table 4 and 5. The total corrosion resistance ( $R_{sum}$ ) is used to represent and evaluate the coating performance (Fig. 10). The corrosion resistance of PPEO-Ca-pH4-SDS is significantly higher compared to that of other coatings, although more amounts of hydroxyapatite are deposited on the surface of PPEO-Ca-pH3-SDS. It can be inferred that the pH value of the post-treatment electrolyte has effect on the corrosion resistance of the composite coatings, since the acidic post-treatment electrolyte also results in the partial dissolution of the composite coating and decrease of corrosion resistance. Moreover, addition of SDS has a huge influence on improvement of the corrosion performance of the coatings, which is probably due to the release and inhibition effect of corrosion inhibitors to the coating/alloy interface when corrosion occurs. Therefore, the corrosion performance of the post-sealed PEO coating is associated with the existence of corrosion inhibitor combined with optimized composition of the post-treatment electrolyte.

### 3.3 Water contact angle

Contact angle measurements are presented in Table 6 and images are gathered in Fig. 11. The value of contact angle obtained for PPEO coating demonstrates the hydrophilic nature of the original oxide layer (i.e.  $<90^\circ$ ) mainly due to its inherent porosity. Coatings sealed at different pH slightly increase the values of contact angle. This might

be associated with the presence of precipitation on the coating surface. The existence of SDS provides hydrophobicity for the coating surface with contact angle up to  $(111 \pm 13^\circ)$  in the case of PPEO-Ca-pH5-SDS. Similar findings were also reported for PEO coatings sealed by ODP acid [27]. Therefore, the obtained results indicate that surface chemistry significantly influences the wettability for these particular layers.

### 3.4 Dry paint adhesion test

The results of the cross-cut paint adhesion test are shown in Fig. 12. The rating system (from 0 to 5) is according to the detached surface (%) after the test considering no detachment (0) and complete detachment (5). Dry paint adhesion tests revealed different features depending on the type of post-treatment process. The rating of PEO coatings without addition of corrosion inhibitors appears to be excellent from the adhesion point of view (as no paint pull-off occurred along the cross-cut lines).

Ca containing precipitates do not have a noticeable effect on paint adhesion. Considering the partial blocking of the pores with Ca containing precipitates, it is believed that the good paintability of the sealed specimens (without SDS) is due to the good adsorption properties of hydroxyapatite. This is in concordance with the hydrophilic character of the layers even after performing post-treatment process. The increase in hydrophobicity of the coatings due to the presence of SDS has a negative influence on the paint adhesion of the layers with rating value up to 4. Only few data are available addressing the paint adhesion of PEO coatings, suggesting that the good adhesion property of the composite layers is ascribed to the outer porous layer [44, 45]. Findings obtained in the present work reveal that modification of the outer porous layer might decrease the adhesion between organic layer and inorganic PEO coating when painting is coated for long-term corrosion protection.

## 4. Conclusions

- 1) The corrosion resistance of PEO coatings on AZ91 Mg alloy can be enhanced by performing sealing post-treatment process. Corrosion inhibitor (SDS) is added into the post-treatment electrolyte to further improve the corrosion performance of the coatings.
- 2) Newly formed Ca containing precipitate, i.e. hydroxyapatite, is deposited on the

original coating surface, which is balanced by the dissolution and redeposition speed during sealing post-treatment process.

- 3) The existence of SDS provides hydrophobicity and inhibition effect for the coating surface, leading to significant improvement of the corrosion performance for PEO coated Mg alloy.
- 4) The increase in hydrophobicity of the PEO coatings treated with SDS has negative influence on the paint adhesion of the layers.

### **Acknowledgements**

The authors would like to acknowledge the financial support from the National Natural Science Foundation of China (NO. 52071067 and 51531007), the Fundamental Research Funds for the Central Universities (N2002009), RTI2018-096391-B-C33 (MCIU/AEI/FEDER, UE) and M. Mohedano is grateful for the support of RYC-2017 21843.

### **Data Availability**

The raw/processed data required to reproduce these findings cannot be shared at this time as the data also forms part of an ongoing study.

### **References**

[1] A.L. Yerokhin, X. Nie, A. Leyland, A. Matthews, S.J. Dowey, Plasma electrolysis for surface engineering, *Surface and Coatings Technology*, 122 (1999) 73-93.

[2] S. Yagi, K. Kuwabara, Y. Fukuta, K. Kubota, E. Matsubara, Formation of self-repairing anodized film on ACM522 magnesium alloy by plasma electrolytic oxidation, *Corrosion Science*, 73 (2013) 188-195.

[3] S. Stojadinović, R. Vasilić, J. Radić-Perić, M. Perić, Characterization of plasma electrolytic oxidation of magnesium alloy AZ31 in alkaline solution containing fluoride, *Surface and Coatings Technology*, 273 (2015) 1-11.

[4] E. Matykina, I. Garcia, R. Arrabal, M. Mohedano, B. Mingo, J. Sancho, M.C. Merino, A.

Pardo, Role of PEO coatings in long-term biodegradation of a Mg alloy, *Applied Surface Science*, 389 (2016) 810-823.

[5] X. Lu, M. Mohedano, C. Blawert, E. Matykina, R. Arrabal, K.U. Kainer, M.L. Zheludkevich, Plasma electrolytic oxidation coatings with particle additions – A review, *Surface and Coatings Technology*, 307, Part C (2016) 1165-1182.

[6] Z.-Q. Zhang, L. Wang, M.-Q. Zeng, R.-C. Zeng, M.B. Kannan, C.-G. Lin, Y.-F. Zheng, Biodegradation behavior of micro-arc oxidation coating on magnesium alloy-from a protein perspective, *Bioactive Materials*, 5 (2020) 398-409.

[7] L.-Y. Cui, H.-P. Liu, W.-L. Zhang, Z.-Z. Han, M.-X. Deng, R.-C. Zeng, S.-Q. Li, Z.-L. Wang, Corrosion resistance of a superhydrophobic micro-arc oxidation coating on Mg-4Li-1Ca alloy, *Journal of Materials Science & Technology*, 33 (2017) 1263-1271.

[8] M. Mohedano, X. Lu, E. Matykina, C. Blawert, R. Arrabal, M.L. Zheludkevich, Plasma Electrolytic Oxidation (PEO) of Metals and Alloys A2 - Wandelt, Klaus, in: *Encyclopedia of Interfacial Chemistry*, Elsevier, Oxford, 2018, pp. 423-438.

[9] G. Barati Darband, M. Aliofkhazraei, P. Hamghalam, N. Valizade, Plasma electrolytic oxidation of magnesium and its alloys: Mechanism, properties and applications, *Journal of Magnesium and Alloys*, 5 (2017) 74-132.

[10] M. Sun, A. Matthews, A. Yerokhin, Plasma electrolytic oxidation coatings on cp-Mg with cerium nitrate and benzotriazole immersion post-treatments, *Surface and Coatings Technology*, 344 (2018) 330-341.

[11] Z. Li, Q. Ren, X. Wang, Q. Kuang, D. Ji, R. Yuan, X. Jing, Effect of phosphate additive on the morphology and anti-corrosion performance of plasma electrolytic oxidation coatings on

magnesium–lithium alloy, *Corrosion Science*, (2019).

[12] S.V. Lamaka, M.F. Montemor, A.F. Galio, M.L. Zheludkevich, C. Trindade, L.F. Dick, M.G.S. Ferreira, Novel hybrid sol–gel coatings for corrosion protection of AZ31B magnesium alloy, *Electrochimica Acta*, 53 (2008) 4773–4783.

[13] S. Wang, X. Guo, Y. Xie, L. Liu, H. Yang, R. Zhu, J. Gong, L. Peng, W. Ding, Preparation of superhydrophobic silica film on Mg–Nd–Zn–Zr magnesium alloy with enhanced corrosion resistance by combining micro-arc oxidation and sol–gel method, *Surface and Coatings Technology*, 213 (2012) 192–201.

[14] Y. Chen, X. Lu, S.V. Lamaka, P. Ju, C. Blawert, T. Zhang, F. Wang, M.L. Zheludkevich, Active protection of Mg alloy by composite PEO coating loaded with corrosion inhibitors, *Applied Surface Science*, 504 (2020) 144462.

[15] S.V. Lamaka, H.B. Xue, N.N.A.H. Meis, A.C.C. Esteves, M.G.S. Ferreira, Fault-tolerant hybrid epoxy-silane coating for corrosion protection of magnesium alloy AZ31, *Progress in Organic Coatings*, 80 (2015) 98–105.

[16] J. Yang, S. Di, C. Blawert, S.V. Lamaka, L. Wang, B. Fu, P. Jiang, L. Wang, M.L. Zheludkevich, Enhanced Wear Performance of Hybrid Epoxy-Ceramic Coatings on Magnesium Substrates, *ACS Applied Materials & Interfaces*, 10 (2018) 30741–30751.

[17] G. Zhang, L. Wu, A. Tang, X. Ding, B. Jiang, A. Atrens, F. Pan, Smart epoxy coating containing zeolites loaded with Ce on a plasma electrolytic oxidation coating on Mg alloy AZ31 for active corrosion protection, *Progress in Organic Coatings*, 132 (2019) 144–147.

[18] M. Toorani, M. Aliofkhazraei, M. Mahdavian, R. Naderi, Superior corrosion protection and adhesion strength of epoxy coating applied on AZ31 magnesium alloy pre-treated by

PEO/Silane with inorganic and organic corrosion inhibitors, *Corrosion Science*, 178 (2021) 109065.

[19] M. Mohedano, C. Blawert, M.L. Zheludkevich, Cerium-based sealing of PEO coated AM50 magnesium alloy, *Surface and Coatings Technology*, 269 (2015) 145-154.

[20] N.V. Phuong, B.R. Fazal, S. Moon, Cerium- and phosphate-based sealing treatments of PEO coated AZ31 Mg alloy, *Surface and Coatings Technology*, 309 (2017) 86-95.

[21] G. Zhang, L. Wu, A. Tang, Y. Ma, G.-L. Song, D. Zheng, B. Jiang, A. Atrens, F. Pan, Active corrosion protection by a smart coating based on a MgAl-layered double hydroxide on a cerium-modified plasma electrolytic oxidation coating on Mg alloy AZ31, *Corrosion Science*, 139 (2018) 370-382.

[22] M. Mohedano, P. Pérez, E. Matykina, B. Pillado, G. Garcés, R. Arrabal, PEO coating with Ce-sealing for corrosion protection of LPSO Mg–Y–Zn alloy, *Surface and Coatings Technology*, 383 (2020) 125253.

[23] L. Pezzato, R. Babbolin, P. Cerchier, M. Marigo, P. Dolcet, M. Dabalà, K. Brunelli, Sealing of PEO coated AZ91magnesium alloy using solutions containing neodymium, *Corrosion Science*, 173 (2020) 108741.

[24] M. Toorani, M. Aliofkhazraei, Review of electrochemical properties of hybrid coating systems on Mg with plasma electrolytic oxidation process as pretreatment, *Surfaces and Interfaces*, 14 (2019) 262-295.

[25] M. Toorani, M. Aliofkhazraei, R. Naderi, M. Golabadi, A. Sabour Rouhaghdam, Role of lanthanum nitrate in protective performance of PEO/epoxy double layer on AZ31 Mg alloy: Electrochemical and thermodynamic investigations, *Journal of Industrial and Engineering*

Chemistry, 53 (2017) 213-227.

[26] C. Liu, X. Lu, Y. Li, Q. Chen, T. Zhang, F. Wang, Influence of post-treatment process on corrosion and wear properties of PEO coatings on AM50 Mg alloy, *Journal of Alloys and Compounds*, 870 (2021) 159462.

[27] B. Mingo, R. Arrabal, M. Mohedano, Y. Llamazares, E. Matykina, A. Yerokhin, A. Pardo, Influence of sealing post-treatments on the corrosion resistance of PEO coated AZ91 magnesium alloy, *Applied Surface Science*, 433 (2018) 653-667.

[28] S.V. Lamaka, B. Vaghefinazari, D. Mei, R.P. Petrauskas, D. Höche, M.L. Zheludkevich, Comprehensive screening of Mg corrosion inhibitors, *Corrosion Science*, 128 (2017) 224-240.

[29] J. Yang, C. Blawert, S.V. Lamaka, K.A. Yasakau, L. Wang, D. Laipple, M. Schieda, S. Di, M.L. Zheludkevich, Corrosion inhibition of pure Mg containing a high level of iron impurity in pH neutral NaCl solution, *Corrosion Science*, 142 (2018) 222-237.

[30] D. Mei, S.V. Lamaka, C. Feiler, M.L. Zheludkevich, The effect of small-molecule bio-relevant organic components at low concentration on the corrosion of commercially pure Mg and Mg-0.8Ca alloy: An overall perspective, *Corrosion Science*, 153 (2019) 258-271.

[31] D. Liu, E.H. Han, Y. Song, D. Shan, Enhancing the self-healing property by adding the synergetic corrosion inhibitors of Na<sub>3</sub>PO<sub>4</sub> and 2-mercaptobenzothiazole into the coating of Mg alloy, *Electrochimica Acta*, 323 (2019) 134796.

[32] L.I. Fockaert, T. Würger, R. Unbehau, B. Boelen, R.H. Meißner, S.V. Lamaka, M.L. Zheludkevich, H. Terryn, J.M.C. Mol, ATR-FTIR in Kretschmann configuration integrated with electrochemical cell as in situ interfacial sensitive tool to study corrosion inhibitors for magnesium substrates, *Electrochimica Acta*, 345 (2020) 136166.

- [33] J. Yang, C. Blawert, S.V. Lamaka, D. Snihirova, X. Lu, S. Di, M.L. Zheludkevich, Corrosion protection properties of inhibitor containing hybrid PEO-epoxy coating on magnesium, *Corrosion Science*, 140 (2018) 99-110.
- [34] Z. Li, Q. Yu, C. Zhang, Y. Liu, J. Liang, D. Wang, F. Zhou, Synergistic effect of hydrophobic film and porous MAO membrane containing alkynol inhibitor for enhanced corrosion resistance of magnesium alloy, *Surface and Coatings Technology*, 357 (2019) 515-525.
- [35] X. Lu, Y. Li, P. Ju, Y. Chen, J. Yang, K. Qian, T. Zhang, F. Wang, Unveiling the inhibition mechanism of an effective inhibitor for AZ91 Mg alloy, *Corrosion Science*, 148 (2019) 264-271.
- [36] Y. Li, X. Lu, K. Wu, L. Yang, T. Zhang, F. Wang, Exploration the inhibition mechanism of sodium dodecyl sulfate on Mg alloy, *Corrosion Science*, 168 (2020) 108559.
- [37] X. Wang, X. Lu, P. Ju, Y. Chen, T. Zhang, F. Wang, Influence of ZnO on thermal control property and corrosion resistance of plasma electrolytic oxidation coatings on Mg alloy, *Surface and Coatings Technology*, 409 (2021) 126905.
- [38] R.H.U. Khan, A. Yerokhin, X. Li, H. Dong, A. Matthews, Surface characterisation of DC plasma electrolytic oxidation treated 6082 aluminium alloy: Effect of current density and electrolyte concentration, *Surface and Coatings Technology*, 205 (2010) 1679-1688.
- [39] M.Y. Koroleva, E.Y. Karakatenko, E.V. Yurtov, Synthesis of Hydroxyapatite Nanoparticles by Controlled Precipitation in the Presence of Sodium Dodecyl Sulfate, *Colloid Journal*, 82 (2020) 275-283.
- [40] H.-L. Yao, H.-T. Wang, X.-B. Bai, G.-C. Ji, Q.-Y. Chen, Improvement in mechanical

properties of nano-structured HA/TiO<sub>2</sub> multilayer coatings deposited by high velocity suspension flame spraying (HVSFS), *Surface and Coatings Technology*, 342 (2018) 94-104.

[41] K. McLeod, S. Kumar, R.S.C. Smart, N. Dutta, N.H. Voelcker, G.I. Anderson, R. Sekel, XPS and bioactivity study of the bisphosphonate pamidronate adsorbed onto plasma sprayed hydroxyapatite coatings, *Applied Surface Science*, 253 (2006) 2644-2651.

[42] L. Wu, L. Zhao, J. Dong, W. Ke, N. Chen, Potentiostatic Conversion of Phosphate Mineral Coating on AZ31 Magnesium Alloy in 0.1MK<sub>2</sub>HPO<sub>4</sub> Solution, *Electrochimica Acta*, 145 (2014) 71-80.

[43] X. Li, S. Deng, H. Fu, G. Mu, N. Zhao, Synergism between rare earth cerium(IV) ion and vanillin on the corrosion of steel in H<sub>2</sub>SO<sub>4</sub> solution: Weight loss, electrochemical, UV–vis, FTIR, XPS, and AFM approaches, *Applied Surface Science*, 254 (2008) 5574-5586.

[44] R. Arrabal, J.M. Mota, A. Criado, A. Pardo, M. Mohedano, E. Matykina, Assessment of duplex coating combining plasma electrolytic oxidation and polymer layer on AZ31 magnesium alloy, *Surface and Coatings Technology*, 206 (2012) 4692-4703.

[45] H. Sharifi, M. Aliofkhazraei, G.B. Darband, S. Shrestha, A REVIEW ON ADHESION STRENGTH OF PEO COATINGS BY SCRATCH TEST METHOD, *Surface Review and Letters*, 25 (2017) 1830004.

[46] P. Sun, Y. Lu, Y. Yuan, X. Jing, M. Zhang, Preparation and characterization of duplex PEO/MoC coatings on Mg–Li alloy, *Surface and Coatings Technology*, 205 (2011) 4500-4506.

[47] U. Malayoglu, K.C. Tekin, S. Shrestha, Influence of post-treatment on the corrosion resistance of PEO coated AM50B and AM60B Mg alloys, *Surface and Coatings Technology*, 205 (2010) 1793-1798.

[48] M. Mohedano, C. Blawert, M.L. Zheludkevich, Cerium-based sealing of PEO coated AM50 magnesium alloy, *Surface and Coatings Technology*, 269 (2015) 145-154.

[49] Z. Li, Y. Yuan, X. Jing, Composite coatings prepared by combined plasma electrolytic oxidation and chemical conversion routes on magnesium-lithium alloy, *Journal of Alloys and Compounds*, 706 (2017) 419-429.

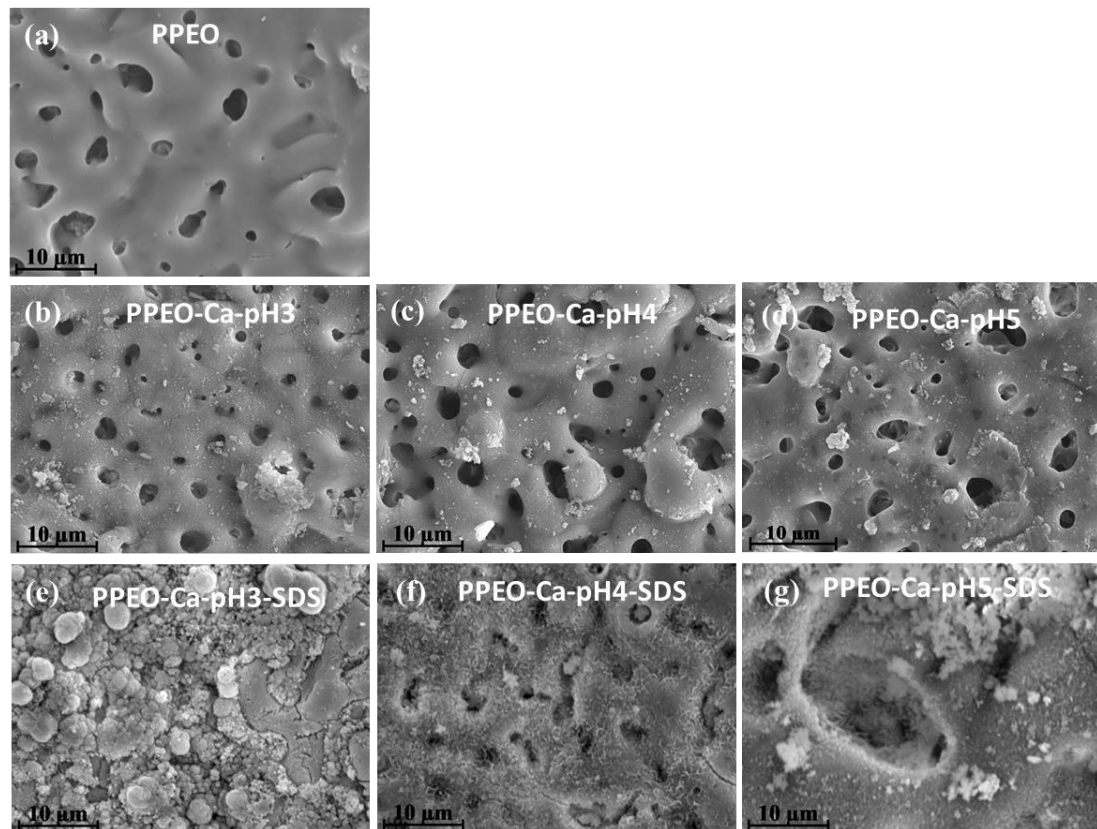


Fig. 1. Surface micrographs of PEO coatings before and after post-treatment in different electrolytes.

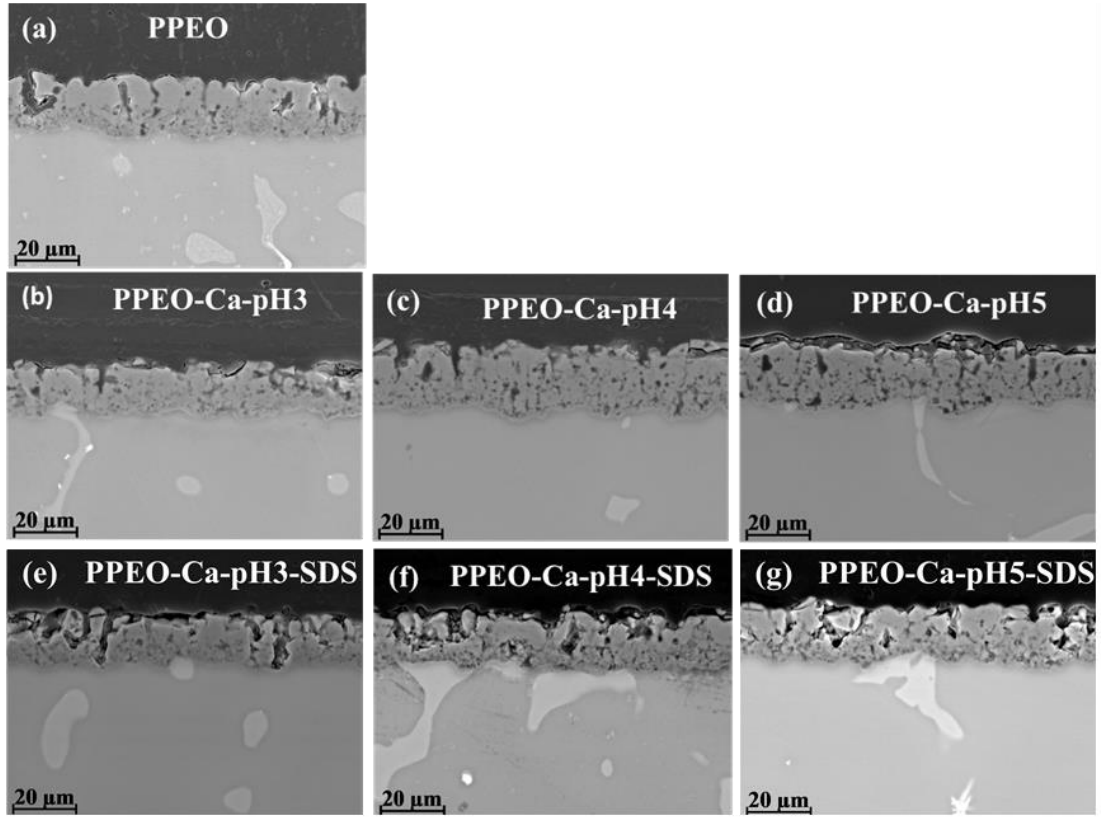


Fig. 2. Cross-sectional micrographs of PEO coated Mg alloy before and after post-treatment in different electrolytes. (a) PPEO:  $(22.7 \pm 1.6) \mu\text{m}$ , (b) PPEO-Ca-pH3:  $(20.1 \pm 1.5) \mu\text{m}$ , (c) PPEO-Ca-pH4:  $(22.5 \pm 1.5) \mu\text{m}$ , (d) PPEO-Ca-pH5:  $(20.5 \pm 1.1) \mu\text{m}$ , (e) PPEO-Ca-pH3-SDS:  $(19.6 \pm 1.3) \mu\text{m}$ , (f) PPEO-Ca-pH4-SDS:  $(21.7 \pm 1.7) \mu\text{m}$ , (g) PPEO-Ca-pH5-SDS:  $(22.5 \pm 2.2) \mu\text{m}$ .

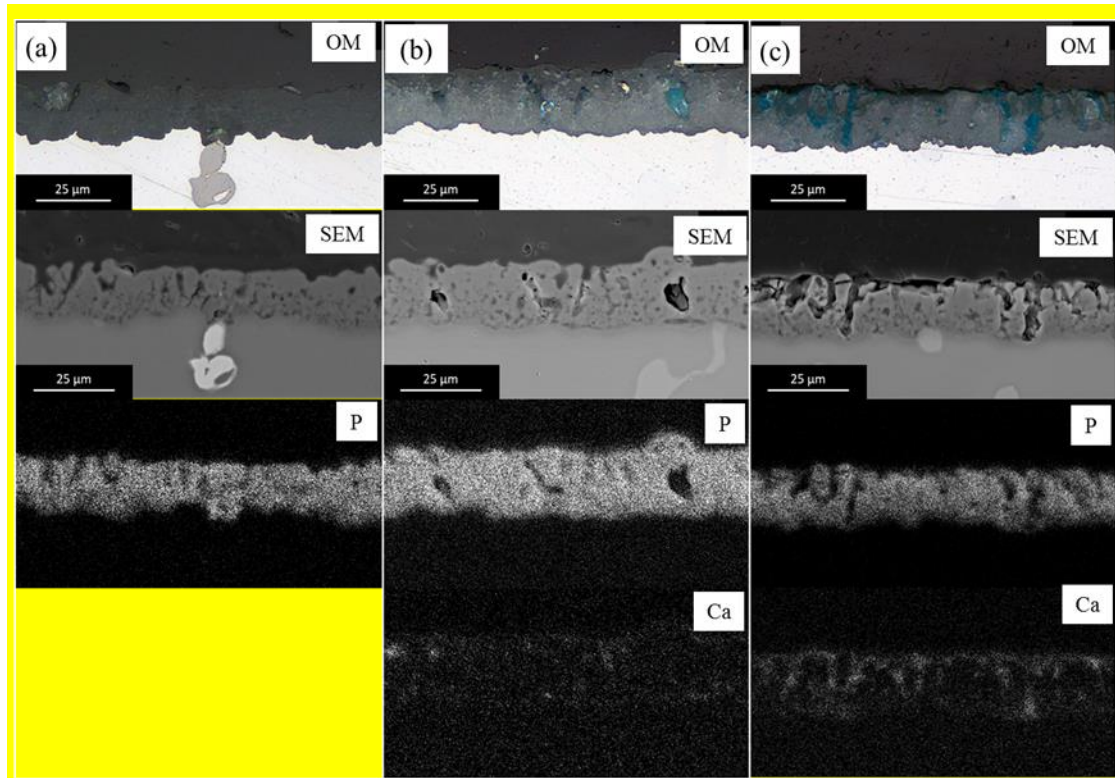
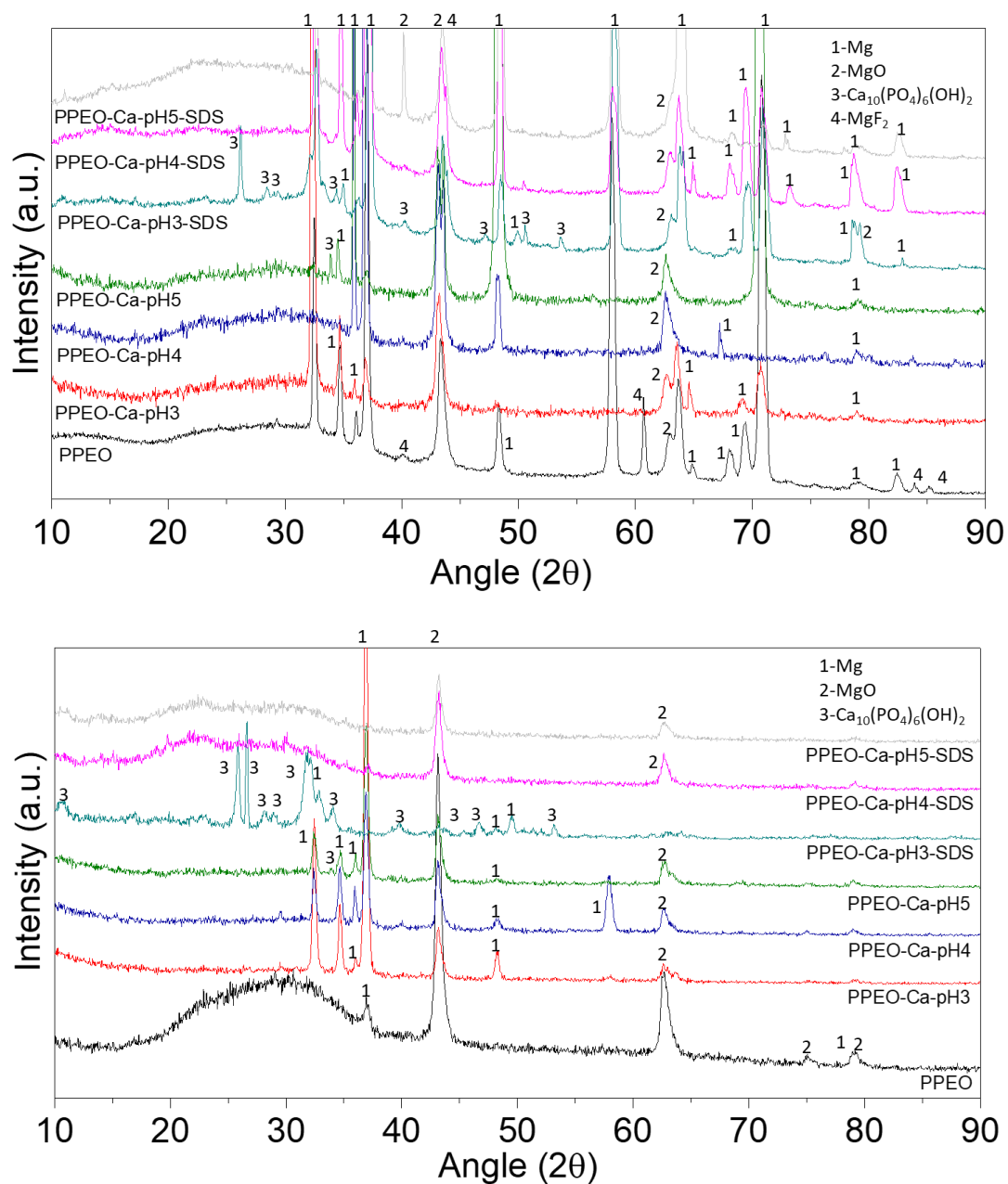
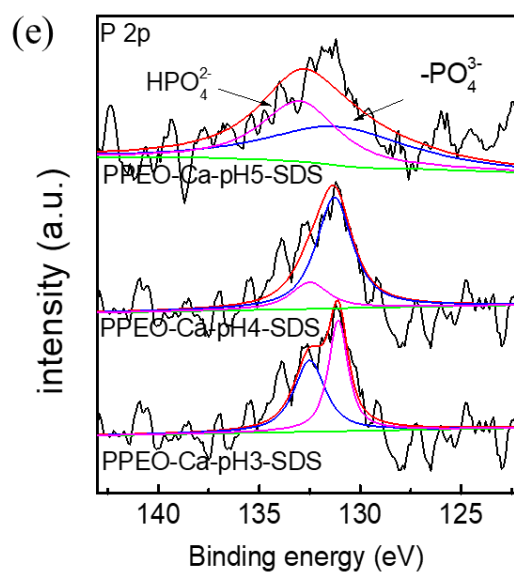
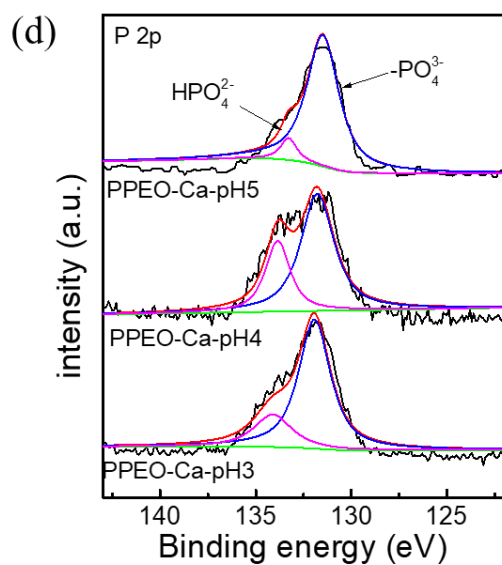
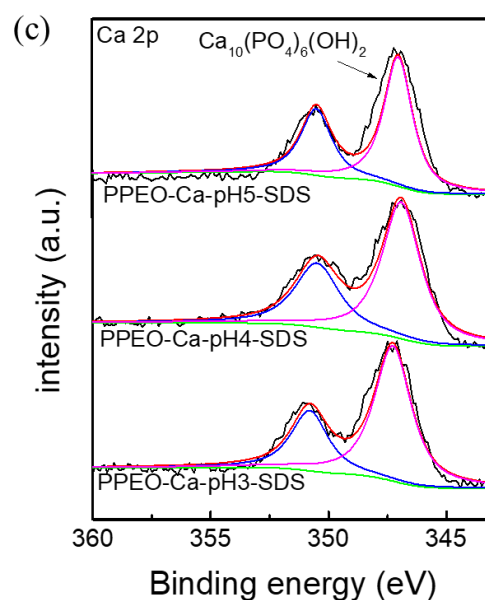
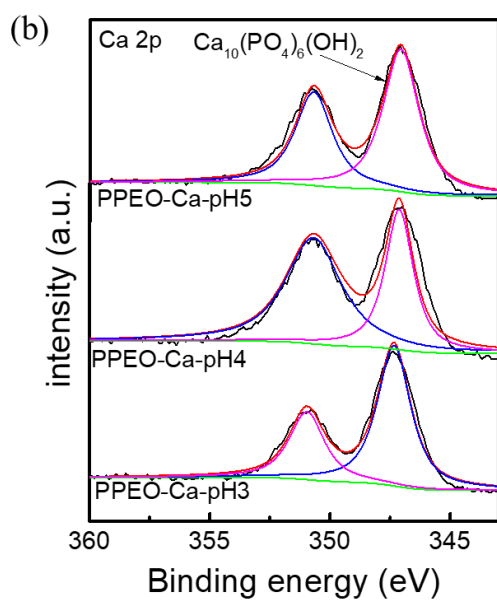
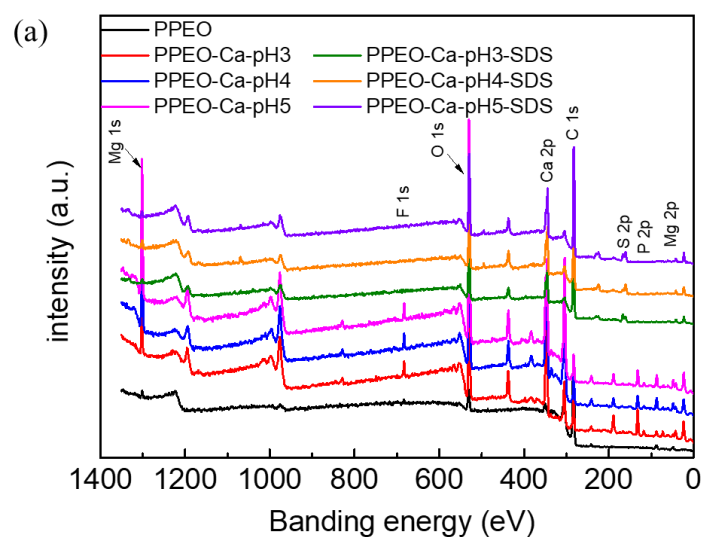
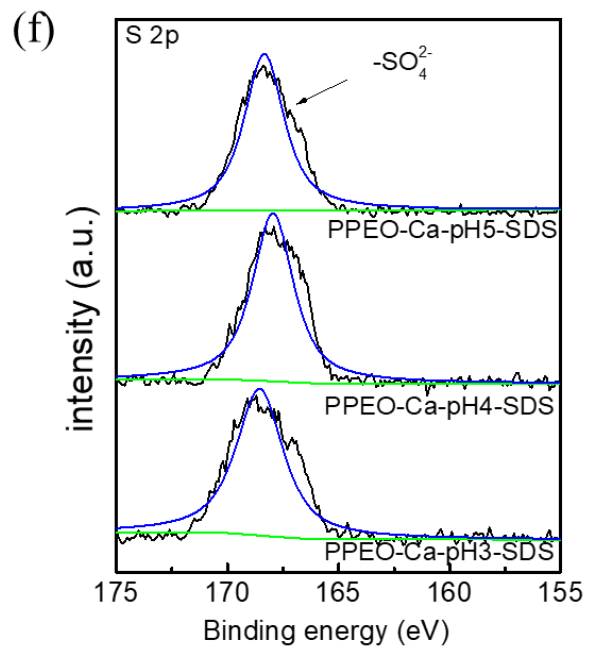


Fig. 3. Cross-sectional micrographs and EDS mappings of PEO coated Mg alloy before and after post-treatment in different electrolytes. (a) PPEO, (b) PPEO-Ca-pH3 and (c) PPEO-Ca-pH3-SDS.



**Fig. 4.** XRD patterns of different coatings (a) Bragg-Brentano, (b) Glancing angle ( $\omega=0.5$ ).





**Fig. 5.** XPS-survey spectra and high-resolution spectra of the coatings. (a) survey spectra, (b) Ca 2p for post-treatment without SDS, (c) Ca 2p for post-treatment with SDS, (d) P 2p for post-treatment without SDS, (e) P 2p for post-treatment with SDS and (f) S 2p for post-treatment with SDS.

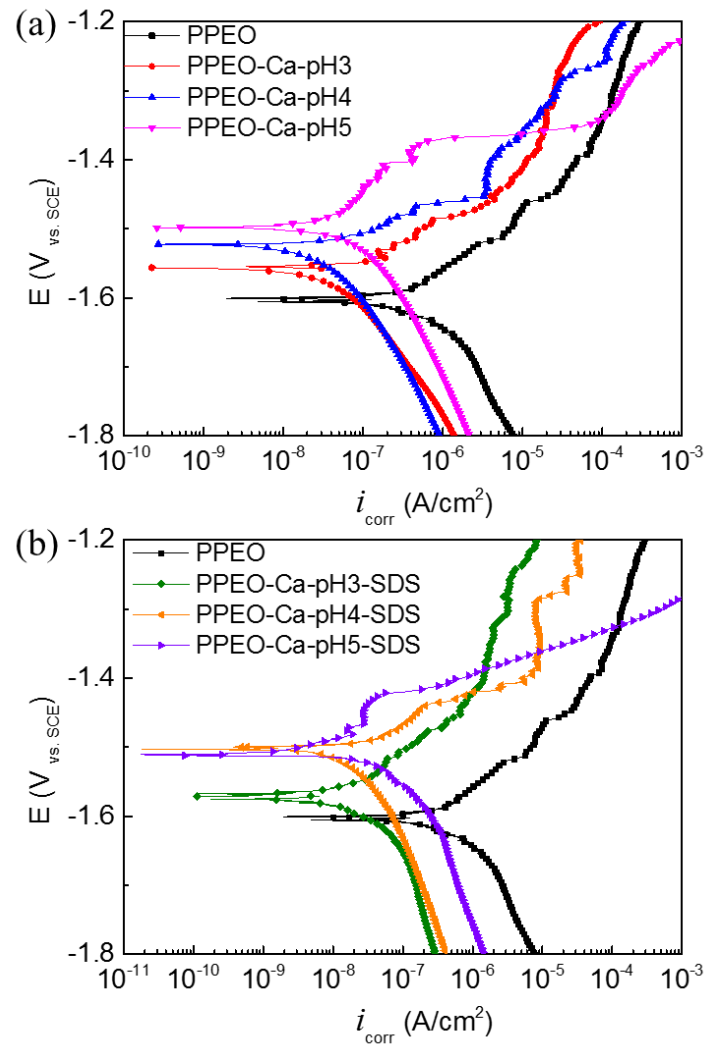


**Fig. 6.** Polarization curves of the coatings in 3.5 wt.% NaCl solution.

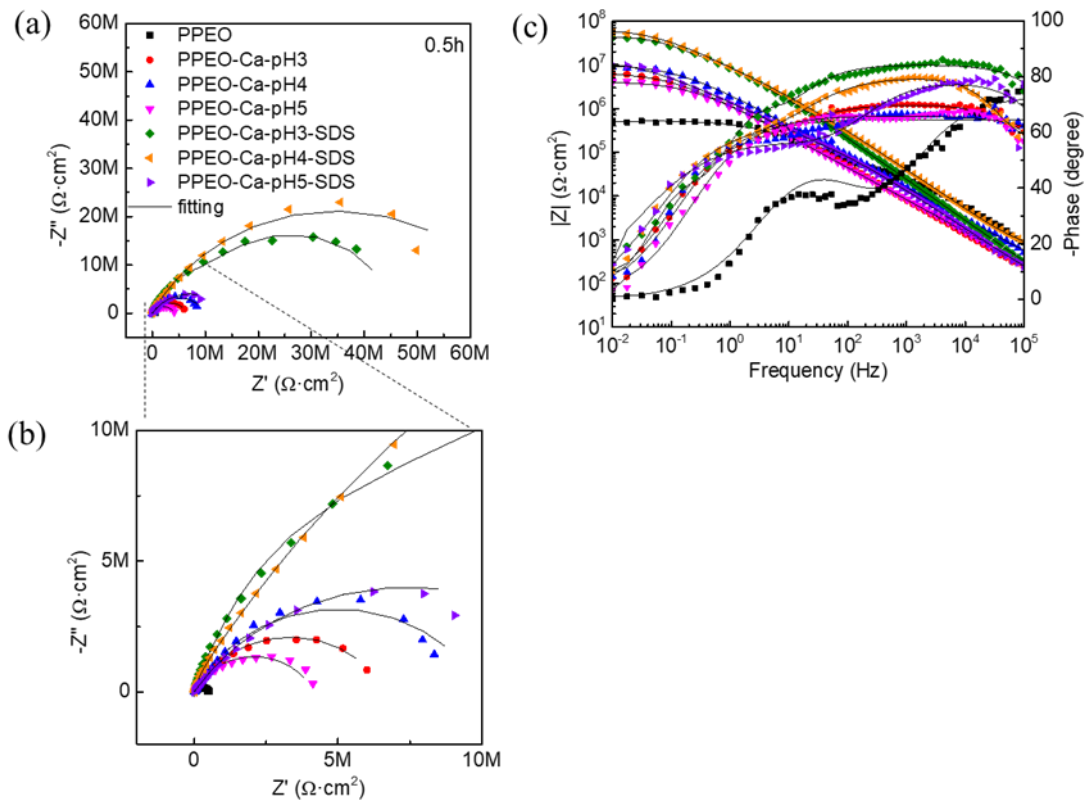


**Fig. 7.** EIS plots of the coatings after immersion 0.5h in 3.5 wt.% NaCl solution. (a) Nyquist plots, (b) enlarged Nyquist plots and (c) Bode plots.

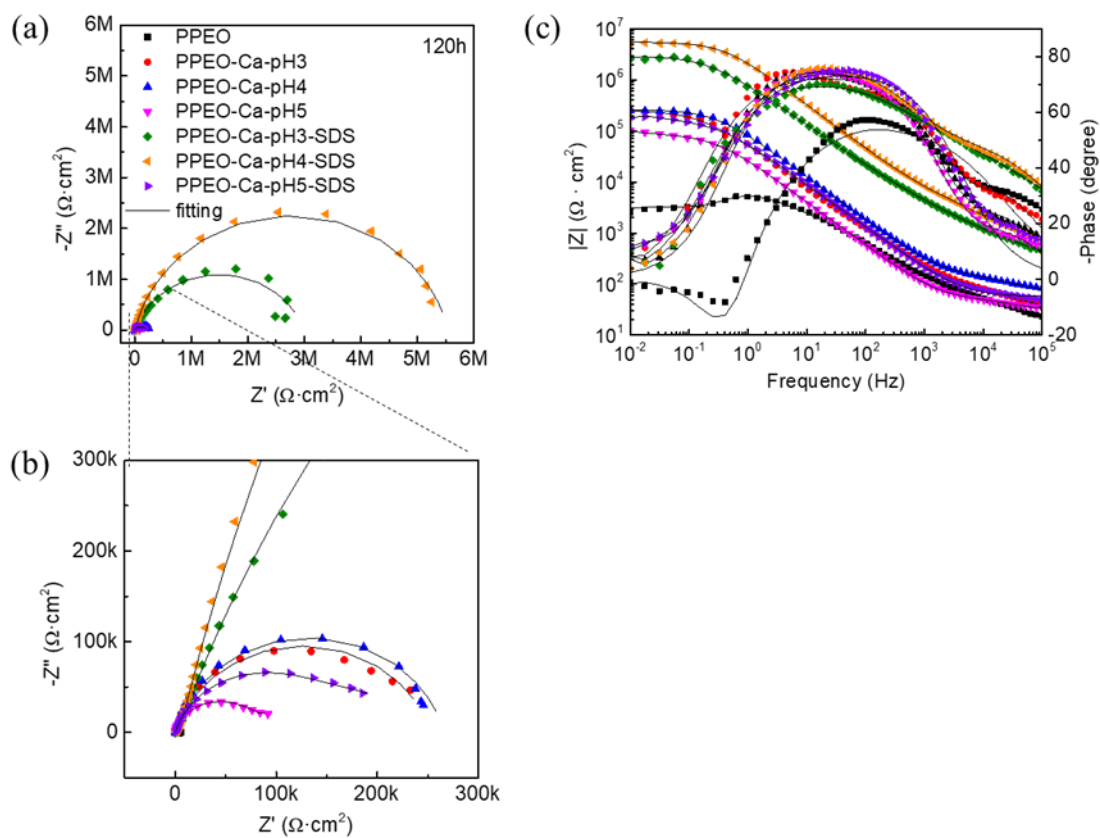


**Fig. 8.** EIS plots of the coatings after immersion 120h in 3.5 wt.% NaCl solution. (a) Nyquist plots, (b) enlarged Nyquist plots and (c) Bode plots.

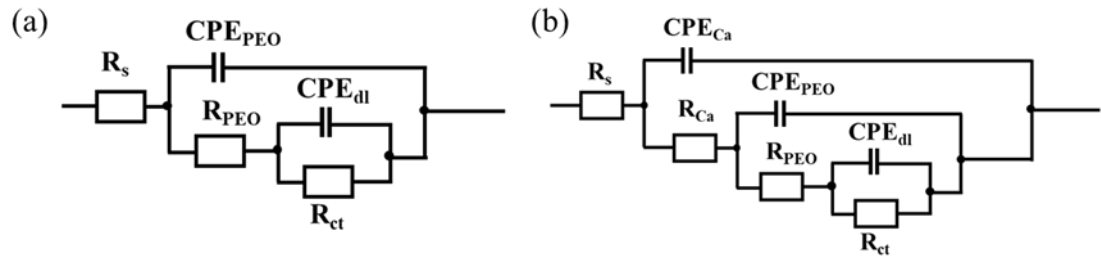


**Fig. 9.** (a) Equivalent circuit used to fit PPEO and PPEO-Ca coatings and (b) equivalent circuit used to fit PPEO-Ca-SDS coatings.

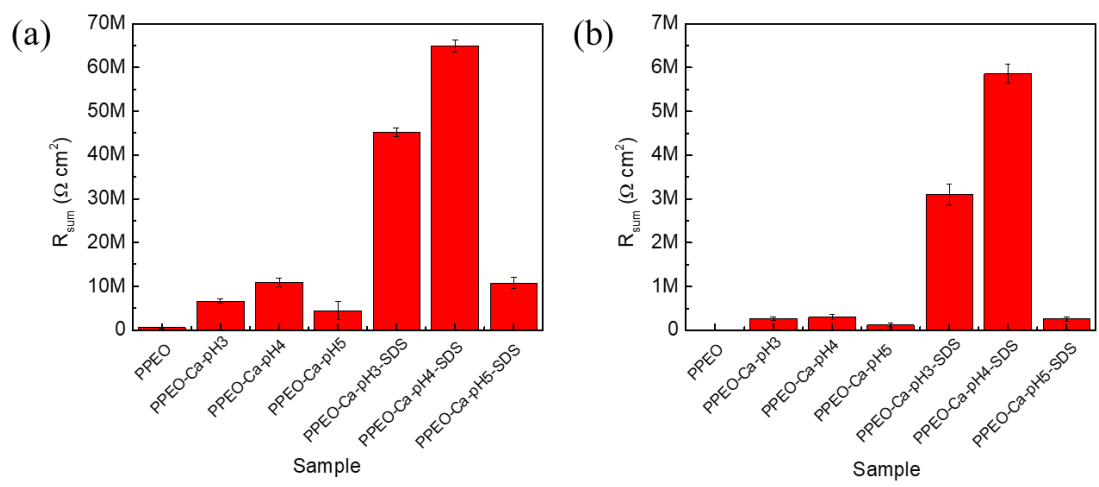


**Fig. 10.**  $R_{sum}$  of different coatings after immersion (a) 0.5 h and (b) 120 h in 3.5 wt.% solution.

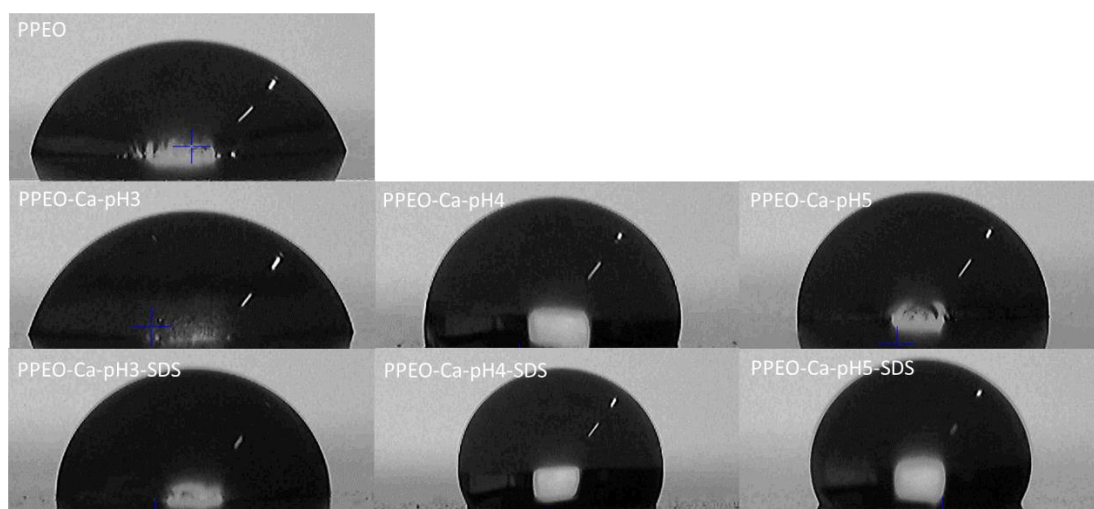


**Fig. 11.** Water contact angle measurement of different coatings.

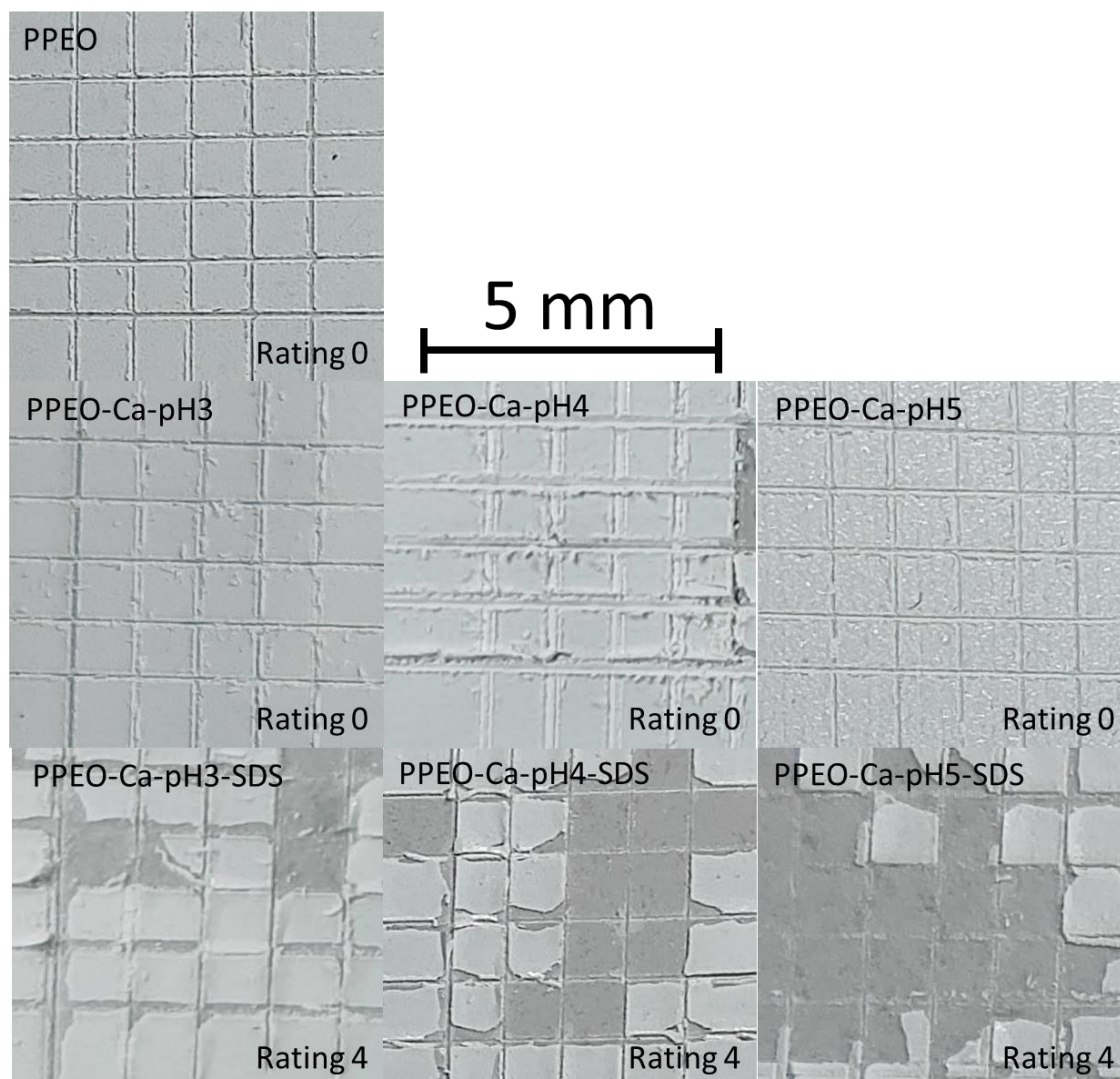


**Fig. 12.** Appearance of painted PEO surfaces after the adhesion test.

Table 1 Summarized information from the publications in terms of PEO coating sealed by inorganic solution.

Mg alloy	Composition of the electrolyte	Sealing process	Corrosion test conditions	Corrosion property	Ref.
Mg-Li alloy	10.0 g/L $\text{Na}_2\text{SiO}_3$ , 3 g/L NaOH and 10 ml/L triethanolamine	20 g/L $\text{Na}_2\text{MoO}_4$ , 4 g/L NaF	Potentiodynamic polarization measurements and EIS. 5 min immersion at 3.5 wt.% NaCl. SCE	$i_{\text{corr}}$ decreases three orders and $E_{\text{corr}}$ increases two orders of magnitude. Impedance increased from 812 to $4.36 \times 10^4 \Omega \text{ cm}^2$	[46]
Mg-Y-Zn alloy	0.086 mol/L $\text{Na}_2\text{SiO}_3$ , 0.15 mol/L NaOH and 0.046 mol/L NaF	10 g/L $\text{Ce}(\text{NO}_3)_3$ , 0.3 g/L $\text{H}_2\text{O}_2$ , 1 g/L $\text{H}_3\text{BO}_3$	Polarization test. 0.5% NaCl SCE	$i_{\text{corr}}$ was reduced from $7.1 \times 10^{-8}$ to $2 \times 10^{-9} \text{ A cm}^{-2}$	[22]
AM50B and AM60B	KOH, $\text{NaAlO}_2$ and $\text{K}_3\text{PO}_4$	12% $\text{KH}_2\text{PO}_4$ and 5% $\text{Na}_2\text{SiO}_3$	Polarization test 3.5% NaCl. SCE	$i_{\text{corr}}$ increased form $10^6 \text{ A cm}^{-2}$ to $10^{-7}$ . $R_p$ was increased from $10^2$ to $10^4 \Omega \text{ cm}^2$	[47]
AM50 Mg	10 g/L $\text{Na}_2\text{SiO}_3$ , 2 g/L KOH	3-10 g/L $\text{Ce}(\text{NO}_3)_3$ , 0.3 g/L $\text{H}_2\text{O}_2$ and 1 g/L $\text{H}_3\text{BO}_3$	EIS. Different times up to 3 days in 0.5% NaCl	Impedance increased from $10^4$ to $6 \Omega \text{ cm}^2$	[48]
Mg-Li alloy	10 g/L $\text{Na}_2\text{SiO}_3$ , 3 g/L NaOH and 10 ml/L triethanolamine	20 g/L $\text{Na}_2\text{SnO}_3$ , 4 g/L NaF, 3 g/L NaOH	Polarization test. 10 min in 3.5% NaCl. SCE	$i_{\text{corr}}$ was reduced from $2.48 \times 10^{-6}$ to $2.94 \text{ A cm}^{-2}$	[49]
AZ91	50 g/L $\text{Na}_2\text{SiO}_3$ , 40 g/L NaOH and 50 g/L $\text{Na}_5\text{P}_3\text{O}_{10}$	12 g/L of $\text{NaNd}(\text{SO}_4)_2$ and 20 mL/L of $\text{H}_2\text{O}_2$	Polarization test and EIS. 1h immersion at 0.1 M $\text{Na}_2\text{SO}_4$ and 0.05 M NaCl. SCE	$i_{\text{corr}}$ reduced from $10^{-6}$ to $10^{-7}$ . Impedance increased from $2.3 \times 10^{-3}$ to $1.3 \times 10^{-4} \Omega \text{ cm}^2$	[23]
AZ31	0.7 M NaOH, 0.1 M NaF, 0.1 M $\text{Na}_3\text{PO}_4$ and 0.1 M $\text{Na}_2\text{SiO}_3$	0.023 M $\text{Ce}(\text{NO}_3)_3 \cdot 6\text{H}_2\text{O}$ and 0.25 M $\text{H}_2\text{O}_2$ at pH = 4 0.1 M $\text{NaH}_2\text{PO}_4$ at pH = 7	Polarization test. 0.5 M NaCl. SCE	$i_{\text{corr}}$ reduced form $1.2 \times 10^{-6}$ to $6.2 \times 10^{-4}$ and $4.9 \times 10^{-4} \text{ A cm}^{-2}$	[20]

Table 2. EDS area analysis of the studied specimens.

Element (at. %)	O	Mg	P	Al	Na	Ca	K	F
PPEO	51.1	27.7	12.2	1.8	2.5	/	0.1	4.6
PPEO-Ca-pH3	55.9	26.4	11.6	2.2	2.6	1	0.2	0.1
PPEO-Ca-pH4	53.2	28.7	12.1	2.1	3	0.5	0.3	0.1
PPEO-Ca-pH5	27.1	43.1	22.7	1.8	3	1.2	0.8	0.2
PPEO-Ca-pH3-SDS	56.2	8.2	14.9	2.1	1	17.4	0.1	0.1
PPEO-Ca-pH4-SDS	52.2	24.6	13.4	2.1	1.5	3.5	0.1	2.5
PPEO-Ca-pH5-SDS	53.8	20.3	14.2	1.1	2.8	4.3	0.4	3

Table 3. Electrochemical data of different coatings obtained from polarization test.

Sample	PPEO	PPEO-Ca- pH3	PPEO-Ca- pH4	PPEO-Ca- pH5	PPEO-Ca- pH3-SDS	PPEO-Ca- pH4-SDS	PPEO-Ca- pH5-SDS
$E_{\text{corr}}$ (V <sub>SCE</sub> )	-1.60	-1.56	-1.52	-1.50	-1.57	-1.50	-1.51
$i_{\text{corr}}$ (μA/cm <sup>2</sup> )	0.572	0.032	0.023	0.085	0.014	0.012	0.028

Table 4. Fitted results of EIS plots of different coatings after immersion 0.5 h in 3.5 wt.% NaCl solution.

Sample	$R_s$ (Ω cm <sup>2</sup> )	$CPE_{Ca}$ (μS s <sup>n</sup> cm <sup>-2</sup> )	n1	$R_{Ca}$ (Ω cm <sup>2</sup> )	$CPE_{PPEO}$ (μS s <sup>n</sup> cm <sup>-2</sup> )	n2	$R_{PPEO}$ (Ω cm <sup>2</sup> )	$CPE_{dl}$ (μS s <sup>n</sup> cm <sup>-2</sup> )	n3	$R_{ct}$ (Ω cm <sup>2</sup> )
PPEO	36.5	—	—	—	21.2	0.81	4.28E4	21.7	0.68	4.90E5
PPEO-Ca-pH3	46.84	—	—	—	13.1	0.78	1.08E6	12.2	0.67	5.54E6

PPEO-Ca-pH4	38.85	—	—	—	12.0	0.72	1.07E7	7.06	0.96	1.56E5
PPEO-Ca-pH5	22.6	—	—	—	19.7	0.73	4.16E6	44.5	0.80	2.36E5
PPEO-Ca-pH3-SDS	37.76	233	0.95	9.73E6	6.25	0.92	3.49E7	3.34	0.94	5.51E5
PPEO-Ca-pH4-SDS	59.3	107	0.86	1.44E7	8.23	0.86	4.67E7	2.21	0.63	3.88E6
PPEO-Ca-pH5-SDS	31.03	132	0.87	6.62E4	24.5	0.83	1.01E7	14.7	0.86	5.73E5

Table 5. Fitted results of EIS plots of different coatings after immersion 120 h in 3.5 wt.% NaCl solution.

Sample	$R_s$ ( $\Omega \text{ cm}^2$ )	$CPE_{Ca}$ ( $\mu\text{S s}^n\text{cm}^{-2}$ )	n1	$R_{Ca}$ ( $\Omega \text{ cm}^2$ )	$CPE_{PEO}$ ( $\mu\text{S s}^n\text{cm}^{-2}$ )	n2	$R_{PEO}$ ( $\Omega \text{ cm}^2$ )	$CPE_{dl}$ ( $\mu\text{S s}^n\text{cm}^{-2}$ )	n3	$R_{ct}$ ( $\Omega \text{ cm}^2$ )
PPEO	21.33	—	—	—	2.19	0.65	3209	22.26	0.88	4216
PPEO-Ca-pH3	32.17	—	—	—	10.88	0.83	2.53E5	2.93	0.82	1.36E4
PPEO-Ca-pH4	33.96	—	—	—	55.5	0.86	2.66E5	1.78	0.84	3.59E4
PPEO-Ca-pH5	25.62	—	—	—	7.53	0.90	6.07E4	24.58	0.72	5.71E4
PPEO-Ca-pH3-SDS	29.23	12.17	0.79	1.64E5	16.22	0.79	2.92E6	71.7	0.82	2.54E4
PPEO-Ca-pH4-SDS	35.2	62.71	0.87	2.97E5	13.32	0.55	5.536E6	57.71	0.78	2.88E4
PPEO-Ca-pH5-SDS	57.09	3.49	0.83	1.65E5	6.72	0.76	7.19E4	15.27	0.82	2.11E4

Table 6. Water contact angle of different coatings.

Sample	Contact angle (°)
PPEO	46±12
PPEO-Ca-pH3	62±3
PPEO-Ca-pH4	52±5
PPEO-Ca-pH5	57±6
PPEO-Ca-pH3-SDS	84±11
PPEO-Ca-pH4-SDS	106±9
PPEO-Ca-pH5-SDS	111±13



**Xiaopeng Lu:** Conceptualization, Investigation, Writing- Reviewing and Editing, Funding acquisition. **Jirui Ma:** Conceptualization, Methodology, Investigation, Writing- Original draft preparation. **Marta Mohedano:** Conceptualization, Investigation, Writing- Reviewing and Editing. **Borja Pillado:** Conceptualization, Investigation, Writing- Reviewing and Editing. **Raúl Arrabal:** Conceptualization, Investigation, Writing- Reviewing and Editing. **Kun Qian:** Conceptualization, Writing- Reviewing and Editing. **Yan Li:** Investigation, Writing- Reviewing and Editing. **Tao Zhang:** Conceptualization, Writing- Reviewing and Editing. **Fuhui Wang:** Conceptualization, Writing- Reviewing and Editing, Supervision, Funding acquisition.

**Declaration of interests**

☒ The authors declare that they have no known competing financial interests or personal relationships that could have appeared to influence the work reported in this paper.

☐The authors declare the following financial interests/personal relationships which may be considered as potential competing interests: